Numerical Simulation of Whistling in Flows around Side-View Mirrors

A. Stoffel, Florent Margnat, C. Prax, F. Vanherpe

Numerical Simulation of Whistling in Flows around Side-View Mirrors

A. Stoffel[1,2], F. Margnat[2], C. Prax[2], F. Vanherpe[1]

1: Stellantis, Centre d'Expertise Métier et Région de Poissy,
2-10 Boulevard de l'Europe, 78300 Poissy, France
2: Institut Pprime - CNRS, Université de Poitiers et ISAE-ENSMA, B17,
6 rue Marcel Doré, TSA 41105, Cedex 9, 86073 Poitiers, France

Abstract: Two side-view mirrors only differing by their caps, whose whistlings were recorded in anechoic wind tunnel during a Hot-Wire Anemometer (HWA) and synchronized microphones campaign, as well as a Time Resolved Particle Image Velocimetry (TR-PIV) and synchronized microphone experiment, are numerically studied. A first study using 2D transient incompressible simulations showed that a normal to the wall random blowing could numerically trigger the whistling generation. 3D transient compressible simulations, representative of the experimental conditions, were then performed using the *PowerFLOW* Lattice Boltzmann Method (LBM) based solver. The general flow topology is well reproduced and matches the experimental data. The whistling source mechanism has been identified for one of the geometries, however, the whistling generation is not captured by the simulation for the other geometry. Therefore, similarly to the 2D simulation, several blowings were applied to the 3D simulation, as an attempt to trigger the whistling generation in a predictive scenario.

Keywords: aeroacoustics, side-view mirror, tonal noise, whistling, Lattice-Boltzmann Method (LBM), random blowing

1. Introduction

The airflow around a side-view mirror may generate whistlings emerging from its broadband aerodynamic noise. Tonal noises are perceived as annoying by the passengers of a car and must therefore be avoided. Werner et. al [1] experimentally demonstrated that the tonal noise emission from side-view mirrors is caused by vortices created upstream the trailing edge, radiating acoustic waves while passing the trailing edge, self-sustaining the creation of vortices in an acoustic feedback loop scenario. Frank et al. [2] were able to confirm this scenario using transient compressible simulations. Nowadays, aerodynamic tonal noise investigation still relies mostly on expensive wind tunnel tests, but the use of numerical methodology could reduce the number of physical test and help preventing whistling sounds at the early design stage.
In the present study, two whistling side-view mirrors that only differ by their caps are studied (figure 1).

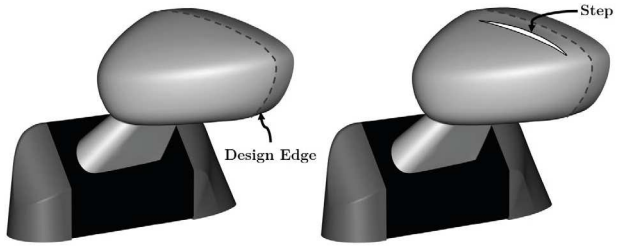

Figure 1: Side-view mirrors designs.

Both side-view mirrors have the same global shape, with a slope change at the Design Edge. The SteppedLine side-view mirror only differs by a step located on the top of its cap and dedicated to turbulence generation in the flow passing by. Therefore, the necessary whistling conditions, i.e. periodic vortex train passing the trailing edge, is avoided downstream the step.
The paper is organised as follows: first, main observations from experimental campaigns are briefly recalled. Secondly, a prior 2D investigation using an incompressible solver is presented in which a normal to the wall blowing is demonstrated to be a good trigger for the whistling source phenomenon. Thirdly, 3D transient compressible simulations, representative of the experimental setup, are performed using Lattice-Boltzmann Method. Finally, blowings are applied to the 3D representative simulations in order to trigger the whistling source mechanism in a predictive scenario.

2. Experimental characterization of the whistlings

Some experimental observations are briefly recalled in this section for contextualising the tonal noise noticed in this study case. In this numerical study, the only free stream velocity investigated is 26 $m.s^{-1}$, with the side-view mirrors at a 15° yaw angle (mirror plane orthogonal to the flow direction). In this case, the flow around the side-view mirrors were experimentally studied using Hot-Wire Anemometer (HWA), as well as Time Resolved Particle Image Velocimetry (TR-PIV), with synchronized microphones for both techniques (figure 2).

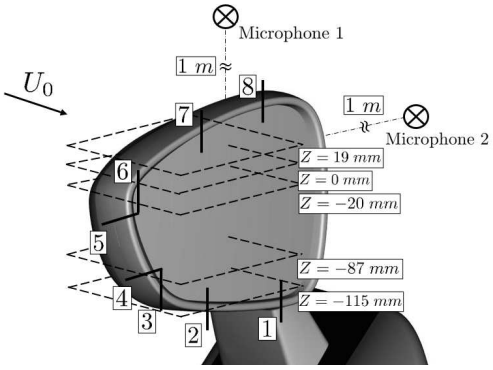

Figure 2: HWA profiles (1 to 8) and TR-PIV planes (noted by their Z-coordinates) recordings locations.

Lazure et al. [3] observed 2 acoustic tonal frequencies for each side-view mirror during the HWA campaign. Stoffel et. al [4] observed similar acoustic characteristics during the TR-PIV campaign (table 1). A third whistling frequency was observed for the SteppedLine side-view mirror, linked to the Whistling Frequency 1 and a ladder-type structure of the tonal noise.

Side-view mirror	Exp.	WF 1	WF 2
BaseLine	HWA	2303	1430
	TR-PIV	2360	1460
SteppedLine	HWA	2165	1437
	TR-PIV	2246	1464

Table 1: Whistlings Frequencies (WF, in Hz) emerging from microphone recordings.

HWA and synchronized microphones postprocessing enabled to locate the whistling sources around the side-view mirror [3] (figure 3). This source locations were confirmed by the TR-PIV field analysis [4]. The dotted white line represents the location where the step suppressed a whistling source.

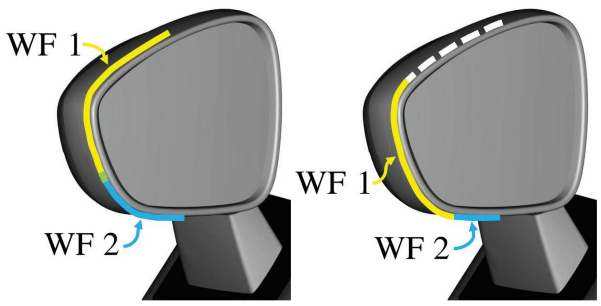

Figure 3: Whistlings sources locations around the side-view mirrors.

3. Transient incompressible 2D simulations

3.1 Numerical methodology

The 2D simulations are performed using a finite differences, direct Navier-Stokes (DNS), incompressible solver, *Incompact3D*. Space derivatives are calculated using a compact, centered scheme of order 6, and temporal marching is performed using a 3rd order Runge-Kutta formulation. An Immersed Boundary Method (IBM) with a forcing term is used for imposing the no-slip condition at the geometry boundary [5].

3.2 2D side-view mirror & cavity tonal noise

The later solver was used to perform a 2D transient, viscous, incompressible simulation of a vertical cut of the BaseLine side-view mirror (figure 4).

Figure 4: 2D vertical cut location of the BaseLine side-view mirror.

For a Re_D of 2000 (based on the height D of the side-view mirror cut), the wake was well established, but no vortex or instabilities that are hold responsible for the tonal noise emission of side-view mirrors upstream the trailing edge are noticed. The use of a splitter plate, such as suggested by Werner et. al [3] in their 2D experimental campaign, yet necessary, was not sufficient to trigger the whistling either.

Nevertheless, a 2D study of cavity tonal noise demonstrated that the incompressible solver is able to predict the frequency of the generated whistling. A good agreement is found in that case between the Strouhal number based on the time series of the velocity fluctuations (St_L) and the Rossiter Strouhal number (St_R) based on the following equation (Eq. 2), for a lot of cases while varying the boundary layer thickness (δ), the cavity length to height ratio (L/D) or the Reynolds number (figure 5), confirming the ability of the incompressible 2D solver to reproduce a pressure driven feedback.

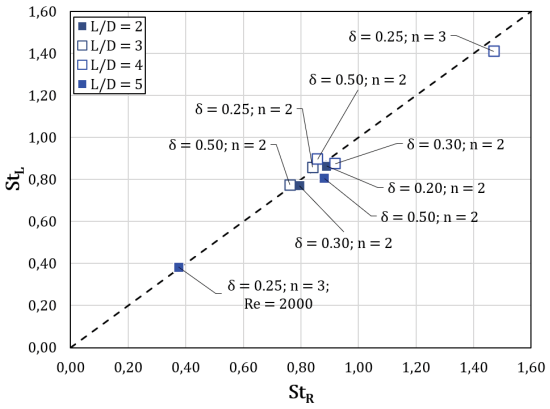

Figure 5: St_L as a function of St_R for several cavity configurations computed using the incompressible solver.

The Strouhal number based on the Rossiter mode is expressed as:

$$St_R = \frac{n-\alpha}{\frac{U_0}{U_c}+M} \qquad [1]$$

With n the mode number, U_0 the free stream velocity, U_c the convection velocity, M the Mach number, and α the phase lag. In low Mach number flows, such as our case, it is reasonable to take $M = 0$, and $\alpha = 0$. Therefore, Eq. 1 becomes:

$$St_R = n\frac{U_c}{U_0} \qquad [2]$$

3.3 The use of blowing to trigger whistlings

In order to stimulate the tonal noise phenomenon, a blowing normal to the surface of the side-view mirror was implemented by modifying the target velocity in IBM. The velocity signal of the blowing is chosen to be random in order to stay in a predictive investigation. It was decided to use a white noise of some % of U_0 with a constant offset. In order to focus on the interested phenomenon, the white noise was low-pass filtered, cutting frequencies higher than $St_D = 10$. Moreover, the blowing started only once the periodic wake was fully established. The location of the blowing is represented by a green arrow in the following figures. The blowing enables an instability wave mode of regular vortices, creating the expected flow for the tonal noise emission of side-view mirrors (figure 6).

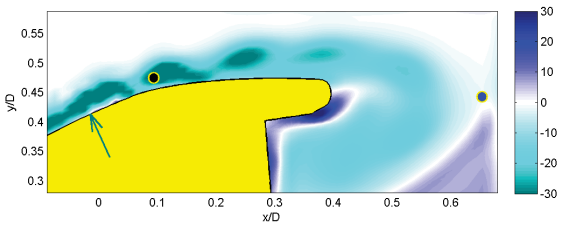

Figure 6: Instantaneous vorticity field of the BaseLine 2D side-view mirror cut while the blowing is implemented.

The time series of the black and the blue probes of figure 6 are shown in figure 7.

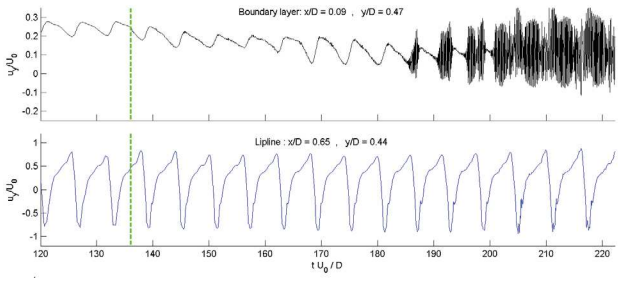

Figure 7: Black and blue probes time signals. The vertical green dotted line represents the start of the blowing.

First of all, time was needed before the blowing triggered the generation of vortices. Then, the vortex generation was being intermittent. In fact, vortices were only born while the u_y component of the wake was high. This characteristic is reached when the wake is high due to its natural flapping, detaching the boundary layer from the wall of the side-view mirror (figure 8).

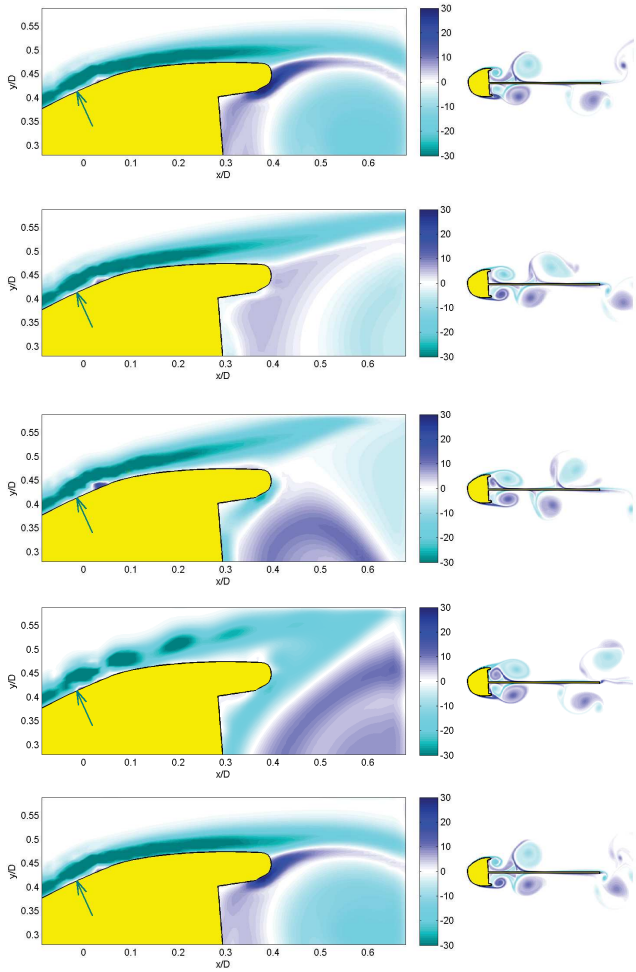

Figure 8: Vorticity field time series of the blowing 2D simulation.

The wake is therefore influencing the boundary layer stability. Indeed, when the wake tends to detach the flow from the wall, the upstream boundary layer is becoming unstable. On the opposite, when the wake tends to reattach the flow to the wall, the boundary layer tends to be more stable.

Figure 9 represents the spectra of the black and the blue probes of figure 6.

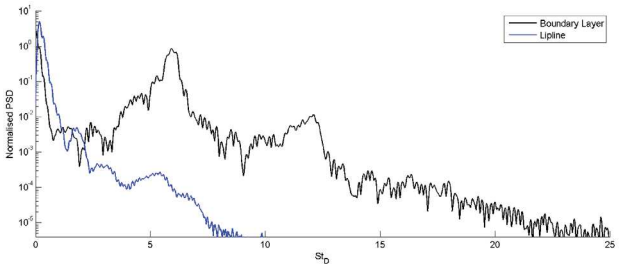

Figure 9: Black and blue probes spectra.

The Strouhal number, normalized by the height of the side-view mirror D, for the periodic vortices generated, is equal to $St_D = 5.92$.

The characteristic length of the resonating phenomenon is proposed to be based on the mean shear layer length from the blowing to the trailing edge. By following this yellow line (figure 10), the length is based on the trajectory of the vortices.

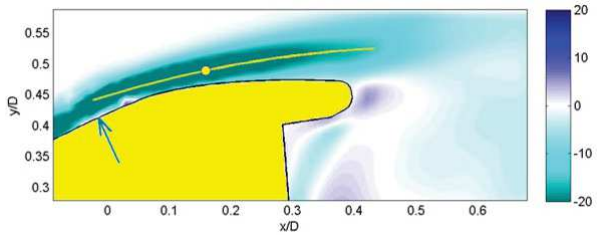

Figure 10: Mean vorticity field of the blowing 2D simulation. The yellow line represents the characteristic length of the whistling phenomenon.

The Strouhal number based on this length is now equal to $St_L = L.St_D = 2.72$. Moreover, the number of vortices n noticed in that length is constant and equal to 4. By analogy to the cavity tonal noise based on Rossiter modes, it is therefore deduced that the mode $n = 4$ seems to be locked. Using Rossiter formula (Eq. 2) with $n = 4$, this Strouhal number is equal to $St_R = 2.96$. The convection velocity has been deduced from cross-correlation between the signal of the black probe of figure 6 and the signal of another moving probe downstream on the vortices path: $U_c \approx 0.74\, U_0$.

The Strouhal number based on Rossiter theory is very close to the Strouhal number based on time signals, confirming the modal locked aspect of such a phenomenon.

4. Representative transient compressible 3D simulations using Lattice Boltzmann Method

4.1 Numerical setup

A transient compressible simulation using the software *PowerFLOW* was performed for both side-view mirrors at a free stream velocity of 26 $m.s^{-1}$. *PowerFLOW* is based on the Lattice Boltzmann Method (LBM), an alternative method relying on microscopic and mesoscopic kinetic equations, instead of classical CFD method based on macroscopic Navier-Stokes equations. In order to reproduce the experimental conditions, the entire BETI wind tunnel was modeled (figure 11) using 13 resolution regions with a minimum voxel size of 0.1 mm (update frequency of 6.06 MHz) in the region of highest resolution. The voxel size is doubling from each region to the next coarser region of lower resolution. The physical simulated time is of 0.206 second for each side-view mirror, for a total cost of around 180 000 CPU hours. Several fluid planes, including the TR-PIV corresponding ones, were stored at a sampling frequency of 20 kHz, while the side-view mirror surface was stored at a sampling frequency of 40 kHz, a box of fluid around the side-view mirror at sampling frequency of 0.4 kHz and 4 microphones at a sampling frequency of 95 kHz. The total stored data represents more than 6 TBytes.

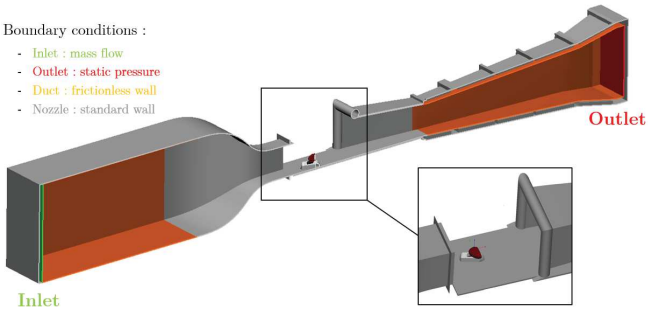

Figure 11: Model setup being representative of the wind tunnel.

4.2 Flow topology results

First of all, the difference between the two geometries influences the flow as expected, being turbulent downstream the step for the SteppedLine side-view mirror compared to the BaseLine side-view mirror (figure 12).

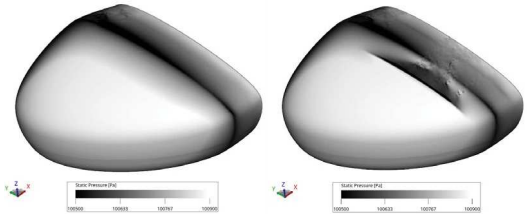

Figure 12: Instantaneous wall pressure for both side-view mirrors.

Moreover, a comparison with averaged TR-PIV planes shows good agreements in terms of averaged flow topology. Two planes are shown in figure 13 for the BaseLine side-view mirror, comparing the time averaged TR-PIV planes, with the time averaged LBM planes, as well as the RANS results obtained for this case [4].

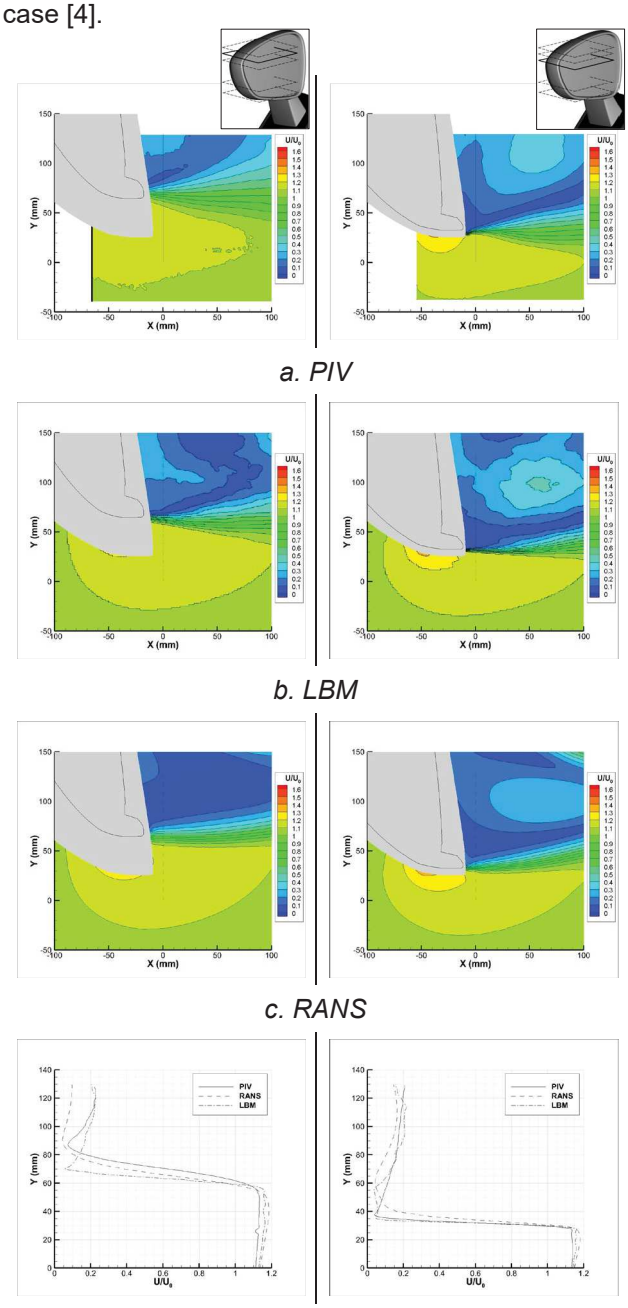

a. PIV

b. LBM

c. RANS

d. Velocity along line

Figure 13: Time averaged PIV, LBM and RANS *Z=0 mm* (left) and *Z=-20 mm* (right) BaseLine plane.

Finally, HWA velocity profiles comparison with the LBM averaged flow velocity and the RANS results is also satisfying (figure 14). The LBM simulations seem more accurate than the RANS model, especially at the step of the SteppedLine (7 profile).

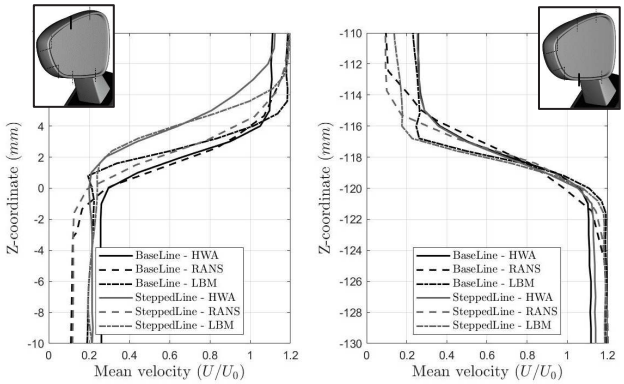

Figure 14: 7 (left) & 2 (right) HWA profiles comparison.

4.3 Whistling scenario observed

A whistling source phenomenon appeared in the SteppedLine simulation. Figure 15 represents the instantaneous Y-velocity fluctuations at the *Z=-20 mm* plane when the expected source of tonal noise was noticed. The time signals of two probes (grey and black points on figure 15), located at the surface of the side-view mirror, are presented on the right side of this figure. A low frequency oscillation is noticed, as well as one burst of high frequency fluctuation, corresponding to the vortices passing by, growing from upstream to downstream location. From these signals, the vortex passing frequency is evaluated to 2143 Hz, very close to the expected whistling frequency.

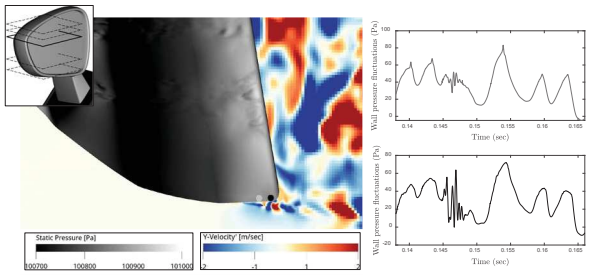

Figure 15: SteppedLine side-view mirror *Z=-20 mm* plane instantaneous Y-velocity fluctuations (left). Wall pressure time signals at 2 locations (right).

The low frequency oscillation noticed in the wall pressure is due to a low frequency flapping of the flow noticed at a fixed location (figure 16). The flow seems to detach and reattach the surface periodically. This low frequency oscillation observed in a fixed plane does not seem to be the cause of the vortex generation, but a consequence of another phenomenon occurring in this scenario. Indeed, the vortex generation location is moving along the surface of the side-view mirror. The vortices are first born downstream the turbulence of the step, then the vortex detachment location moves slowly along the surface of the side-view mirror towards its external side (following the black arrow on figure 17).

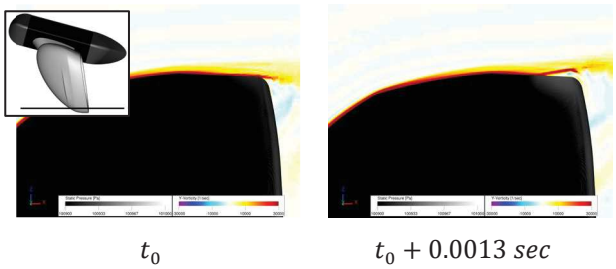

t_0 $t_0 + 0.0013\ sec$

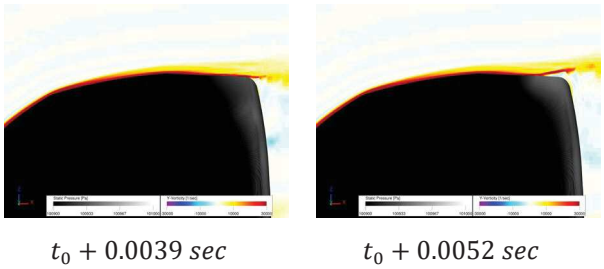

$t_0 + 0.0039\ sec$ $t_0 + 0.0052\ sec$

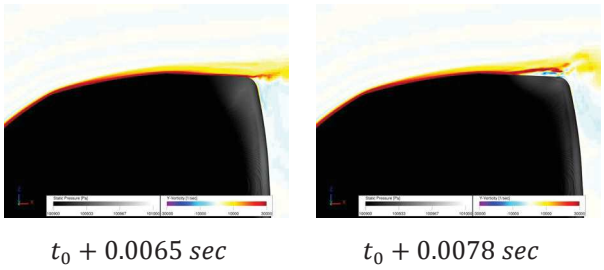

$t_0 + 0.0065\ sec$ $t_0 + 0.0078\ sec$

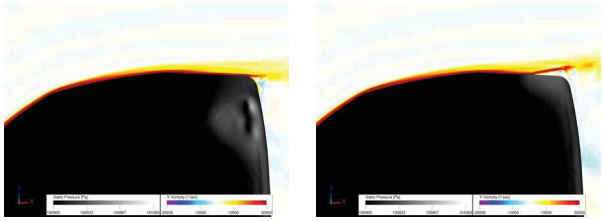

$t_0 + 0.0117\ sec$ $t_0 + 0.0156\ sec$

Figure 16: Time series of Y-Vorticity in a vertical plane for the SteppedLine simulation.

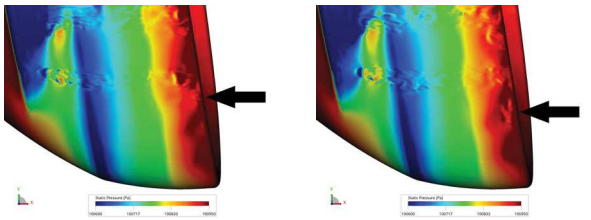

$t_0 + 0.0026\ sec$ $t_0 + 0.0052\ sec$

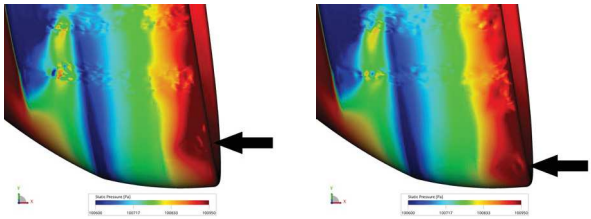

$t_0 + 0.0078\ sec$ $t_0 + 0.0104\ sec$

Figure 17: Wall pressure snapshots from the top view of the SteppedLine simulation.

This transport of the vortices along the surface being seen as a low frequency oscillation must be link to an intermittency of vortex generation. If vortices were created continuously, at a fixed location, nothing else could be seen. In order to confirm this hypothesis, the wall pressure fluctuations along the black line of figure 18 are shown on figure 19 in the time and frequency domains. The distance axis is the projection of the curvilinear black line in the gray horizontal line of figure 18.

Figure 18: Line along the trailing edge of the side-view mirror used for wall pressure fluctuations extraction.

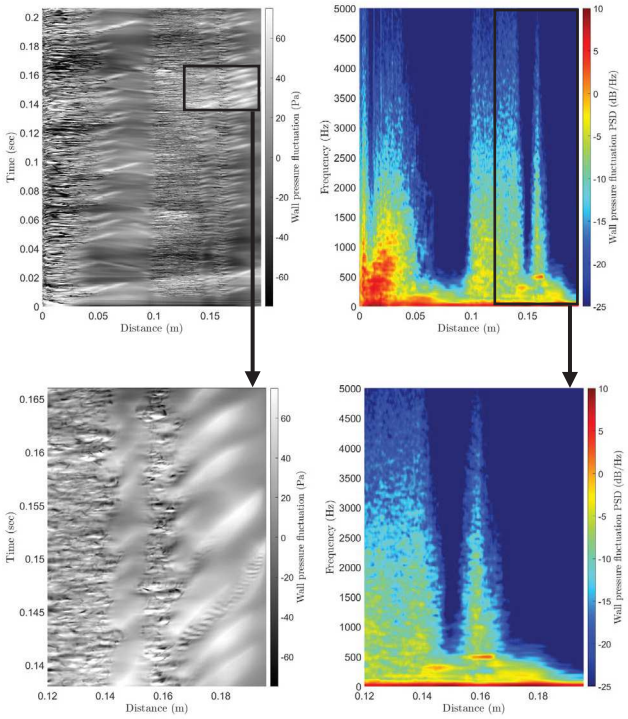

Figure 19: Wall pressure fluctuations along the side-view mirror line in the time domain (left) and in the frequency domain (right).

The turbulent flow downstream the step is well noticeable between approximately 0.1 and 0.15 m, as well as overpressure lines, born at turbulent location, and being transported along the black line, towards the external side of the side-view mirror. Zooming in this figure, the high frequency whistling source phenomenon is observed again and is transported along this black line. This vortex generation lasted therefore much longer than what only noticed at a fixed probe. Several tonal sources phenomena are noticed, but not all of them are generating vortices for

such a long time. Indeed, other tonal phenomenon are noticed near the turbulence, but do not last long. In the frequency domain, at the turbulent location where the whistling source is born (0.16 m), a clear peak at around 500 Hz is emerging, corresponding to the intermittency of the vortex generation, seen as a low frequency oscillation in a fixed location and discrete overpressure moving along the black line in this figure.

Following a vortex detachment along its transport in the time domain yields to the signal shown in figure 20. From this time signal, a vortex passing frequency of around 2300 Hz is found, close to the expected tonal frequency again.

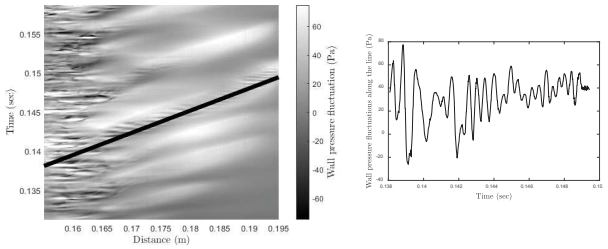

Figure 20: Line following the vortex detachment transport along the surface (left), and the wall pressure fluctuation associated (right).

Finally, the following scenario is deduced from this simulation (figure 21): The vortex detachment is born downstream the turbulent flow of the step and is generating vortices that are convected by the flow, passing the trailing edge of the side-view mirror at the whistling frequency (high velocity). At the same time, the vortex detachment location is moving along the trailing edge at a low velocity resulting in seeing “vortex packets” being transported along the trailing edge, continuously generating vortices convected by the mean flow. The intermittence of such packets creation results in a low frequency oscillation of the flow at a fixed plane, of around 500 Hz. This scenario for the SteppedLine whistling is consistent with the experiments since a low frequency intermittency of vortex generation of the same order was noticed in the *Z=-20 mm* fixed plane using TR-PIV [4].

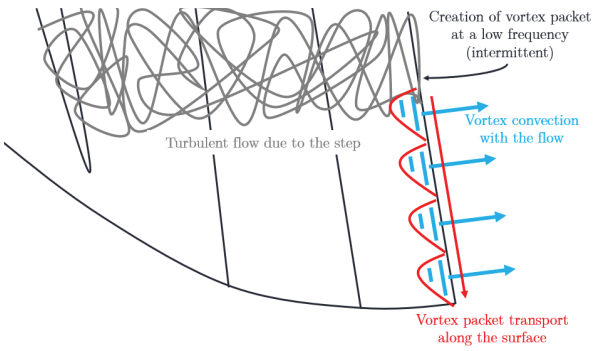

Figure 21: SteppedLine whistling scenario.

The Baseline simulation did not show any sign of whistling. The mesh and the setup being able to reproduce such small vortices near the wall for the SteppedLine simulation evidences nevertheless that the numerical apparatus is well adapted for the tonal noise investigation.

5. Blowings applied to the 3D simulations using Lattice Boltzmann Method

5.1 Blowing signals and locations

In order to trigger the whistlings in the LBM simulations, two blowings at two locations are investigated, resulting in a total of 4 cases (table 2).

	Design Edge	**Secondary Edge**
Signal 1	BaseLine	BaseLine
Signal 2	BaseLine	SteppedLine

Table 2: Blowing cases for the LBM investigation.

Two different time signals are used, with and without a constant offset, both based on white noise random signal filtered with a low pass filter that cut off frequencies higher than 4000 Hz (figure 22).

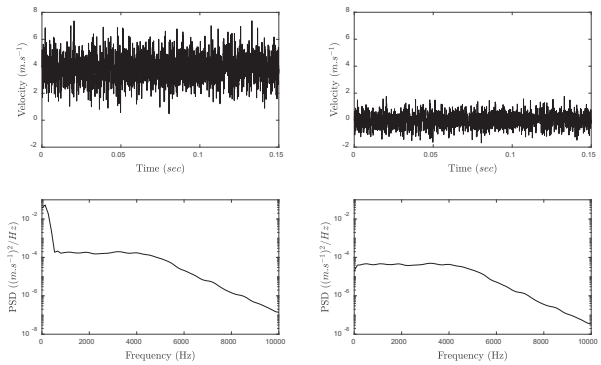

Signal 1 *Signal 2*

Figure 22: Blowings inlet time signals and their spectra.

All of the blowings are applied normal to the surface, all around the side-view mirrors, parallel to the trailing edge, with a thickness of 1 mm, at two different locations. One location is near the Design Edge, and the other further downstream, at a Secondary Edge (white lines on figure 23).

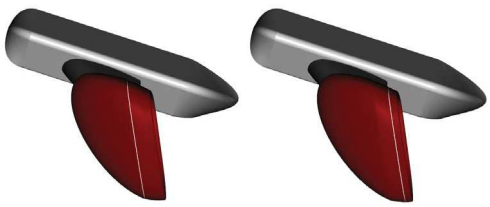

Figure 23: Blowing locations. Design Edge (left), Secondary Edge (right).

5.2 Blowing results

Despite the 500 000 CPU hours used, and the 13 TBytes of data stored, this blowing technique did not lead to whistling flow situations. Hence, a best practice for the simulation of tonal noise emission in the case of side-view mirrors is hard to find. First of all, the blowing in a compressible simulation will result in adding a strong acoustic source in the pressure field at the blowing location (figure 24).

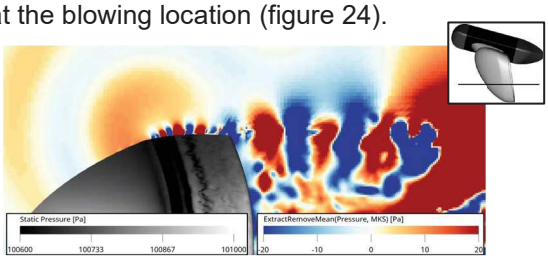

Figure 24: Instantaneous pressure fluctuations field in a blowing simulation.

Moreover, a strong blowing can result in a vectorised jet at the surface of the side-view mirror, instead of being a boundary layer trigger (figure 25.b). Some instabilities from the blowing result in a fully turbulent boundary layer instead of a frequency selected instability (figure 25.a). Weaker blowing generates tiny fluctuations that are convected within the flow without disturbing it enough (figure 25.c, 25.d). Last but not least, all flows return to a steady state when the blowing stopped.

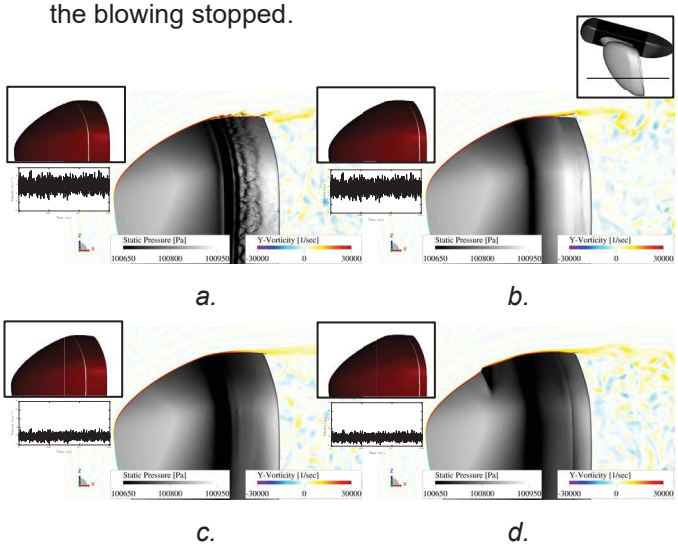

Figure 25: Instantaneous Y-vorticity and wall pressure for each blowing case.

6. Conclusion

Normal to the wall random blowing has been able to trigger the whistling source phenomenon in a 2D transient incompressible simulation. The responsible vortices are locked analogically to a Rossiter mode and are generated intermittently since the wake flapping is strongly influencing the boundary layer stability. 3D simulations using *PowerFLOW,* representative of the experiment, allow reproducing the global flow topology and bring many informations on the whistling source phenomenon for the SteppedLine side-view mirror. The flow transitioned to turbulent at the step of the SteppedLine simulation, and good agreements with experimental averaged flow are shown. The whistling source phenomenon was identified in the SteppedLine simulation, at a frequency close to the measured one. The vortex detachment seems to be born at the turbulence of the step, and then moves along the surface. These moving vortices are seen with a low frequency oscillation at a fixed plane since they are intermittently born at the turbulence, where a low frequency peak is emerging in the wall pressure spectrum. Nevertheless, whistling did not appear in the BaseLine simulation, making the use of such simulations for tonal noise prediction not satisfying. Finally, a predictive whistling simulation best practice using 3D compressible simulations, even triggered by blowings, is hard to find. Despite lots of resources used, several phenomenon appeared in the blowing simulations such as strong monopole in the pressure field, or transition to turbulent flow upstream the trailing edge, but the expected tonal noise source phenomenon was not captured.

7. References

[1] M.J. Werner, W. Würz & E. Krämer: *"Experimental investigation of an aeroacoustic feedback mechanism on a two-dimensional side mirror model."*, Journal of Sound and Vibration, 387 :79-95, 2017.

[2] H. M. Frank & C.-D. Munz: *"Direct aeroacoustic simulation of acoustic feedback phenomena on a side-view mirror."*, Journal of Sound and Vibration, 371 :132-149, 2016.

[3] H. Lazure, V. Morinière, J. Laumonier & L. Philippon: "*Sifflement aérodynamique d'un rétroviseur*", 13ème Congrès Français d'Acoustique, Le Mans, France, 2016.

[4] A. Stoffel, F. Margnat, C. Prax & F. Vanherpe: "*Experimental and Numerical Analysis of Whistling in Flows around Side-View Mirrors*", 16ème Congrès Français d'Acoustique, Marseille, France, 2022.

[5] F. Margnat & V. Morinière: *"Behaviour of an immersed boundary method in unsteady flows over sharp-edged bodies."*, Computers & fluids, 38(6): 1065-1079, 2009.

8. Glossary

CFD: Computational Fluid Dynamics
LBM: Lattice Boltzmann Method
IBM: Immersed Boundary Method
HWA: Hot-Wire Anemometer
TR-PIV: Time Resolved-Particle Image Velocimetry

This work was realized in the course of a PhD as part of a convention (CIFRE) between the Association Nationale de la Recherche et de la Technologie (ANRT) and the automotive company Stellantis.